J. Fluid Mech. (1992), *vol.* 242, *pp.* 299–321
Printed in Great Britain

Vortex shedding from slender cones at low Reynolds numbers

By A. PAPANGELOU

Department of Engineering, University of Cambridge, Trumpington Street, Cambridge CB2 1PZ, UK

(Received 12 November 1991 and in revised form 17 February 1992)

Wind-tunnel experiments on the flows created by a number of slightly tapered models of circular cross-section have shown the presence of spanwise cells (regions of constant shedding frequency) at Reynolds numbers of the order of 100. The experiments have also shown a number of other interesting features of these flows: the cellular flow configuration is dependent on the base Reynolds number and independent of the tip Reynolds number, the frequency jump between adjacent cells is a function of flow speed, taper angle and kinematic viscosity, but is constant along a cone's span, and the unsteady hot-wire anemometer signal is both amplitude and phase modulated. A mathematical model is proposed based on the complex Landau–Stuart equation with a spanwise diffusive coupling term. Numerical solutions of this equation have shown many of the qualitative features observed in the experiments.

1. Introduction

Although the problem of the flow past a circular cylinder has received a great deal of attention (see Williamson 1989 for a very good introduction to the subject), very little has been done to study flows over other bodies of revolution. The dependence of the vortex shedding frequency on Reynolds number raises interesting questions about how the frequency might vary along a body of slowly changing diameter (and, by implication, changing local Reynolds number). Gaster (1969, 1971) addressed this problem. Using cones with relatively high taper angles (18:1 and 36:1), Gaster (1969) observed local shedding frequencies lower than those for a circular cylinder of the same diameter. His signals were modulated by a low-frequency oscillation that was independent of any lengthscale, and he went on to propose a theoretical model involving a spanwise-coupled nonlinear oscillator. Later, experiments on the flow over a cone of much smaller taper angle (Gaster 1971) showed the presence of spanwise cells (regions of constant frequency) along the cone. The results showed how the spanwise coupling inherent in such a system could significantly alter the resulting flow pattern.

More recently, Piccirillo (1990) has also investigated the shedding from a tapered body. He observed spanwise cells positioned symmetrically along the cone, and found that the vortex shedding geometry was largely unaffected by end conditions. Noack, Ohle & Eckelmann (1991) have proposed a mathematical model for the formation of such cells based on the van der Pol oscillator first proposed by Gaster (1969). They also presented experimental results for one cone.

The research presented here was undertaken in order to extend Gaster's early work on slender cones of circular section. A number of cones of varying taper angle were

Cone	Length (mm)	Base diameter (mm)	Tip diameter (mm)	Taper angle (mrad)
A	202	2.19	1.85	0.842
B	202	2.31	1.81	1.238
C	202	2.57	1.55	2.525
D	202	2.86	1.36	3.713
E	202	3.08	0.98	5.198
F	200	3.15	0	7.875

TABLE 1. The dimensions of the cones.
(The taper angle is defined as the semi-vertex angle of the cone.)

used in the experiments. The experimental results are presented in §3, and in §4 a mathematical model for the vortex system is proposed. The model yields many of the qualitative features of the experimentally determined flow.

2. Experimental details

Table 1 shows the dimensions of the six stainless steel cones used in the experiments. Most experiments were conducted with cones A, C, and F, as these adequately covered the broad spectrum of possible flow regimes. Endplates of 15 and 10 mm diameter were constructed for the 'base' (or root) and 'tip' of the cones, respectively. Measurements of velocity fluctuations were made 10–15 mm downstream of the cones using a miniature hot wire of the boundary-layer type connected to a DISA 55D05 battery-operated constant-temperature anemometer, the output of which was amplified and low-pass filtered. Signals were sampled at 400 Hz by a Plessey SPM02 Spectrum Analyser interfaced to an Acorn Archimedes 310 computer. The turbulence level of the wind tunnel (12 in. × 12 in. in cross-section) was less than 0.15%, whilst flow uniformity was better than 0.8%.

Air speeds in the tunnel, of the order of 1 m/s, were determined using a calibrated vortex-shedding device described by Papangelou (1992).

3. Experimental results

3.1. *Existence of cellular regime*

Figure 1 shows time series of the hot-wire signal for cone C obtained at various spanwise positions, z, determined as the distance from the base of the cone. A maximum Reynolds number, $Re_{\max}$, may be defined as the Reynolds number at the base of the cone, and a local Reynolds number, Re_{loc}, may be defined for all other spanwise locations. Near the base end ($z = 50$ mm, figure 1*a*), the signal resembles a sine wave, maintaining a constant *dominant* frequency component with changing spanwise location, z, despite small changes in Re_{loc}. As z increases the signal becomes progressively more modulated ($z = 85$ mm, figure 1*b*). At some value of z ($z = 100$ mm, figure 1*c*), the modulation of the amplitude is largest and phase jumps are occasionally observed. Some irregularity is also apparent in the signals. For larger z ($z = 105$ mm, 110 mm, figure 1 (*d* and *e*)) the modulation decreases, though from now on it is always present, and a new (higher) frequency dominates. It is this variation in the dominant shedding frequency component along the cone that results in the cellular structure of the flow. It is important to stress that each signal seems

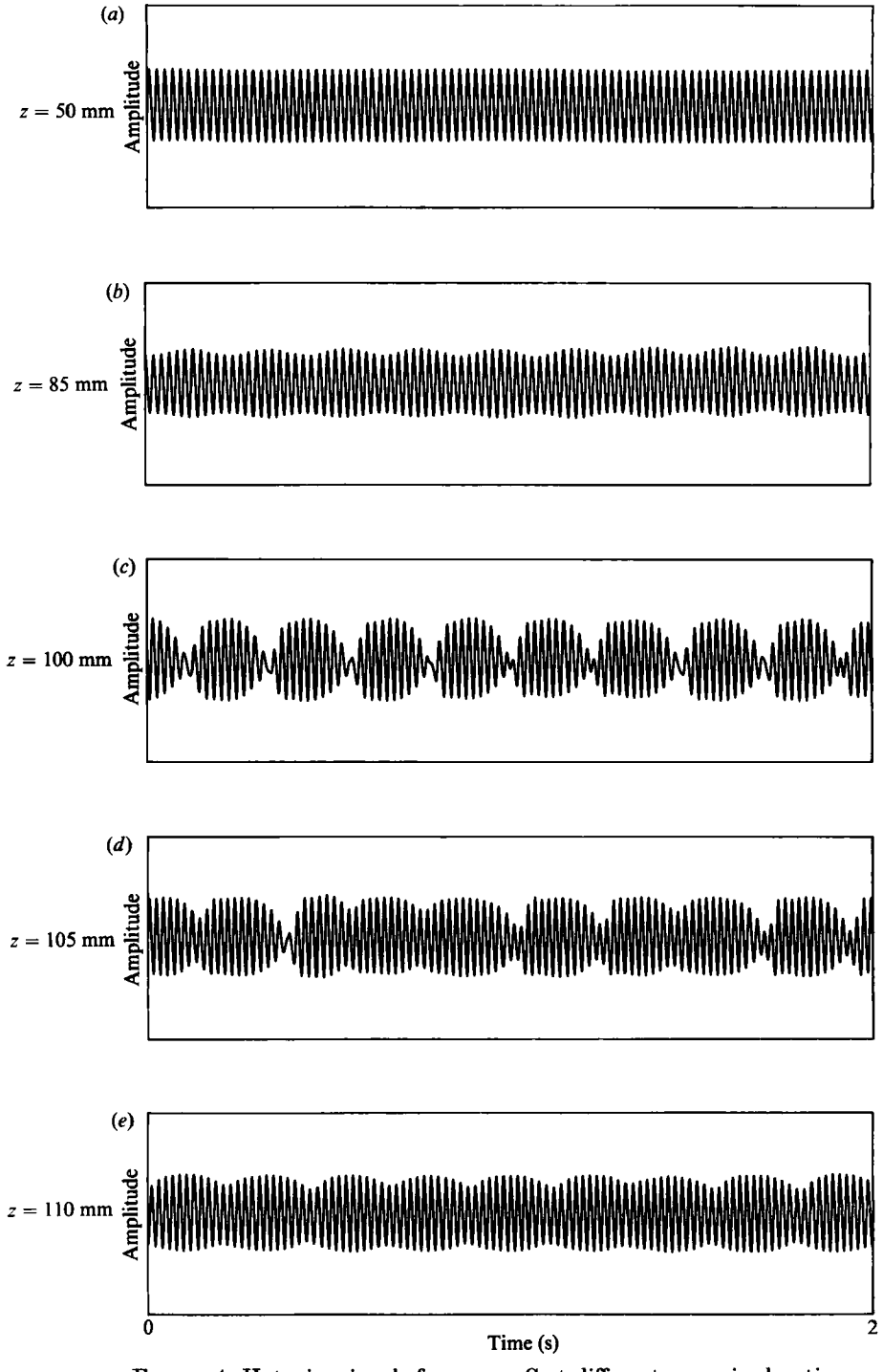

FIGURE 1. Hot-wire signals from cone C at different spanwise locations, z.

to be composed of a number of different frequency components and that the concept of a cell, for the time being, is based on the behaviour of the most dominant frequency component. The modulation frequency of the signals is observed to be of the same magnitude as the difference between the two dominant frequency components of adjacent cells.

By locating the dominant frequency in the power spectrum at a number of spanwise locations, it was possible to characterize the different experimental flow regimes that exist. Figure 2 shows a number of different flow regimes obtained in this way. The Roshko line, defined as the shedding frequency for a circular cylinder of the same local diameter, is also shown. Roshko (1954) determined this line from his experiments as

$$Ro = 0.212Re - 4.5 \quad (50 < Re < 150),$$

where the Roshko number, $Ro = fd^2/\nu$, is a non-dimensionalized frequency based on diameter, d, shedding frequency, f, and kinematic viscosity, ν.

At the lowest Reynolds numbers ($Re < 80$) no distinct cells are observed. Instead, there is a 'pre-cellular' regime characterized by a continuously increasing frequency (figure 2*a*). The hot-wire signal is strongly modulated along the whole length of the cone. Such a continuous variation in frequency is possible only if modulation is present. It is this process of modulation that allows coherent vortices to be shed at different rates along the cone. Gaster (1969) also observed strong modulation and a continuously varying frequency for cones of much higher taper angles. The trend in the frequency variation of figure 2(*a*) is similar to that of Roshko, but all the frequencies lie below his line. No vortex shedding was observed for points $z > 170$ mm, corresponding to Reynolds numbers less than about 50, a typical value for the critical Reynolds number.

At higher Reynolds numbers ($Re \approx 100$) a 'cellular' regime emerges, in which spanwise regions of constant dominant frequency are present. Figure 2(*b*) shows how the cells begin to form at the base end (where Reynolds numbers are largest), creating a situation where both cellular and pre-cellular regimes may co-exist. Figure 2(*c*) shows a purely cellular regime (obtained by a further increase in Reynolds number) consisting of four distinct cells (of progressively smaller size) in addition to the usual end cells. All the points lie below Roshko's line, and the frequency jump between adjacent cells is constant.

At still higher Reynolds numbers ($Re > 150$), the cellular regime begins to break down. Figure 2(*d*) shows how this breakdown begins, significantly, at the tip, where the Reynolds numbers are lowest. The region closest to the base appears to be more resilient, despite its larger local Reynolds numbers, and is the last to break down. This observation, combined with the earlier observation that the cellular regime also emerges at the base end, suggests that the two ends of the cone have different roles to play. This will be confirmed later. At still higher Reynolds numbers the signals become less regular, and a 'post-cellular' regime emerges as shown in figure 2(*e*).

Except for the end cells, only one cell was present along the whole length of cone A (smallest taper angle), as illustrated by figure 2(*f*). Figure 2(*g*) shows a multiple-cell configuration for cone F (largest taper angle). After the first three or four cells, the cells become too indistinct for any meaningful observations to be made. Vortices are shed by cone F in the cellular regime at Reynolds numbers as low as 25, which is well below the usual critical Reynolds number for the onset of vortex shedding. This is due to strong spanwise coupling which induces vortices near the tip. Interestingly, the lowest Reynolds number at which Sreenivasan, Strykowski &

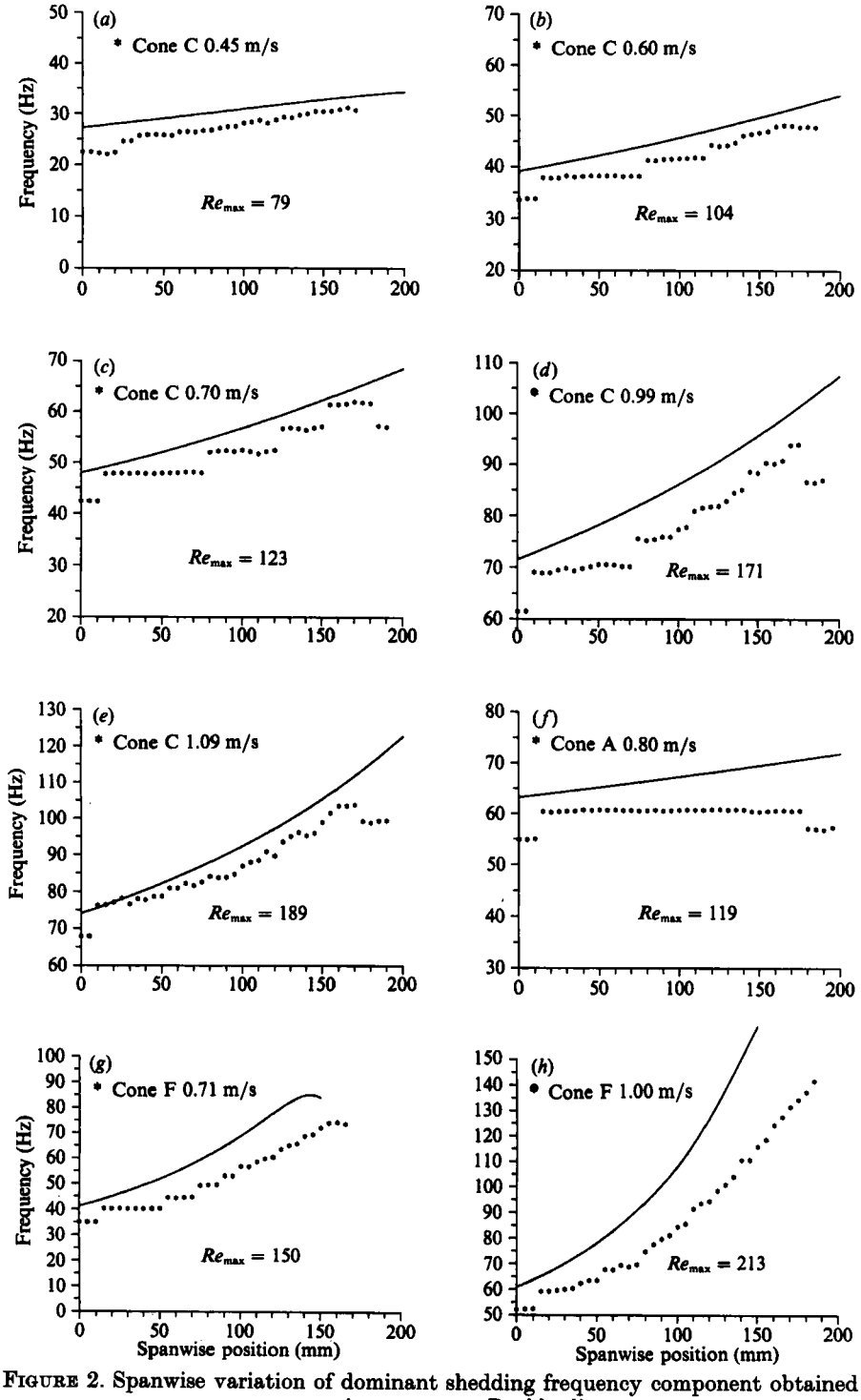

FIGURE 2. Spanwise variation of dominant shedding frequency component obtained from experiments. ——, Roshko line.

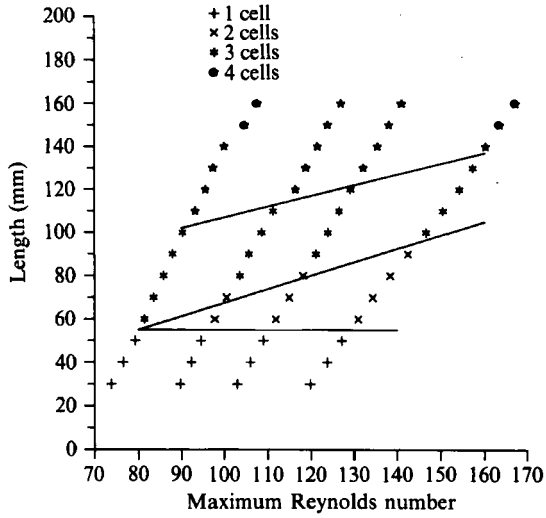

FIGURE 3. The influence of cone length and maximum Reynolds number on number of cells. Cone C.

Olinger (1987) managed to induce shedding (by acoustic excitation) was very similar ('about 25'). Finally, figure 2(*h*) shows the post-cellular configuration for cone F.

3.2. *Variation of flow configuration*

The dependence of a cell's frequency on the model geometry was investigated using the single-cell case of cone A. By using movable endplates at both ends, the available spanwise length of the cone was varied whilst the shedding frequency was monitored. The results showed that there was no discernible change in cell frequency when the endplate at the tip end was moved. This suggested that the cell's frequency was determined by the largest diameter, and this was confirmed by subsequent experiments involving the movement of the base endplate. This lack of influence of the tip endplate was also noted by Piccirillo (1990), but he failed to investigate the effect of a movement of the base endplate. It became clear that the tip endplate causes only a local disturbance to the flow, while movement of the base endplate has a more global influence.

In order to investigate the dependence of a multiple-cell flow configuration on geometry, the cell boundaries of cone C were identified for various combinations of geometry and speed. Figure 3 shows the number of cells observed as a function of cone length, l, and maximum Reynolds number, $Re_{\max}$. Each point corresponds to one experiment, and the solid lines indicate the boundaries between different cellular configurations. An increase in length clearly allows more cells to exist, but the most interesting observation is that the number of cells for a given geometrical arrangement has a tendency to decrease with increasing air speed, suggesting an increase in spanwise coupling. For small cone lengths, the low-aspect-ratio configuration supported only one cell and this resulted in the horizontal line which separates the one-cell and two-cell regimes. Similar one-cell configurations at low aspect ratios have been observed by Gerich & Eckelmann (1982), Papangelou (1992) and others.

Attention was subsequently directed to the jump between a three-cell and a two-cell regime caused by an increase (or decrease) in flow speed. The extreme sensitivity of the system, combined with the practical difficulties of maintaining the system at

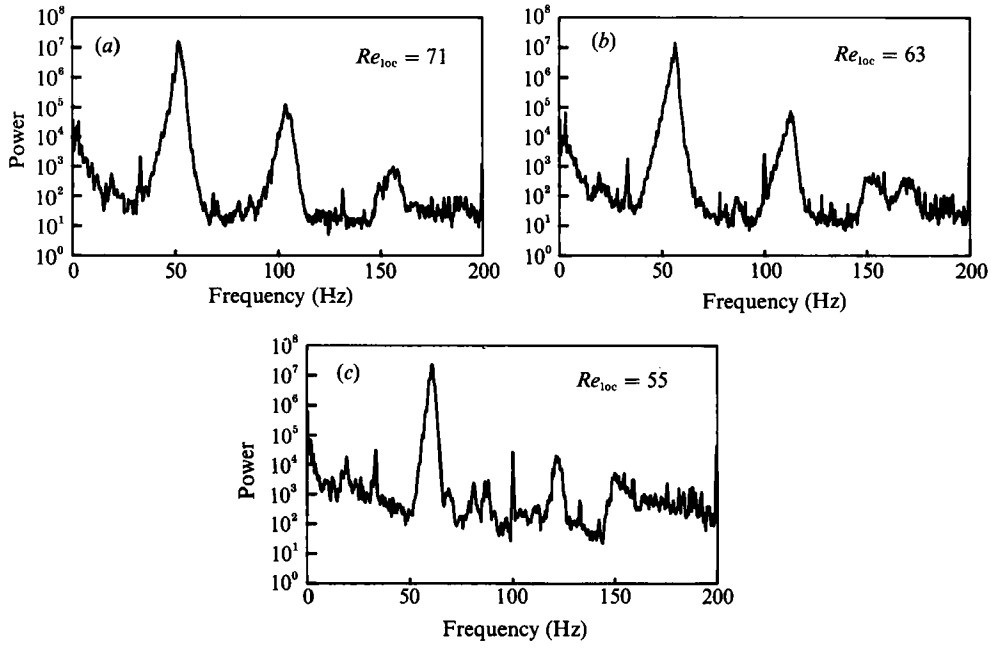

FIGURE 4. Power spectra at pre-cellular Reynolds numbers ($Re < 80$).
Cone C (*a*) $z = 50$ mm; (*b*) $z = 100$ mm; (*c*) $z = 150$ mm.

a precisely constant speed for sufficiently long periods of time, made the characterization of this jump difficult. Hysteresis could be neither identified nor ruled out with any confidence. However, it was established that the jump occurred with the simple disappearance (or appearance) of one of the cells rather than with the formation of an entirely new cellular configuration. It will be seen in §4.3 that this agrees well with the mathematical model, and with the results of Noack *et al.* (1991) who also concluded that 'the birth of a cell is a local event which does not lead to global changes along the span'.

The progressively decreasing size of the cells along the span of a cone (as shown in figure 2*c*) may be explained as follows. Assume that each spanwise point has some 'natural' shedding frequency (attained in the absence of any spanwise coupling) associated with it, such as that given by the Roshko line. As the local diameter varies along the length of the cone, the coupled frequency (within a cell) departs more and more from the local 'natural' frequency, and the 'strain' on the system's coupling increases. When the difference between the two frequencies is large enough, there is a jump to a higher frequency corresponding to that of the next cell. Since this jump was observed to be of constant magnitude along the length of the cone (this will be discussed in §3.4), the progressively steeper incline of the 'natural' frequency curve (with spanwise location) results in progressively smaller cells. The concept of a 'strain' leading to cells (in cylinder vortex shedding) has also been proposed by König, Eisenlohr & Eckelmann (1990), who associated it with the local shedding angles. The present observations differ from those of Piccirillo (1990) who observed equally sized cells.

3.3. *Power spectra*

At the lowest Reynolds numbers the power spectrum features a broad peak whose centre frequency varies continuously along the length of the cone. Figure 4 shows a series of such pre-cellular spectra for cone C. It is clear that there is no distinct single-

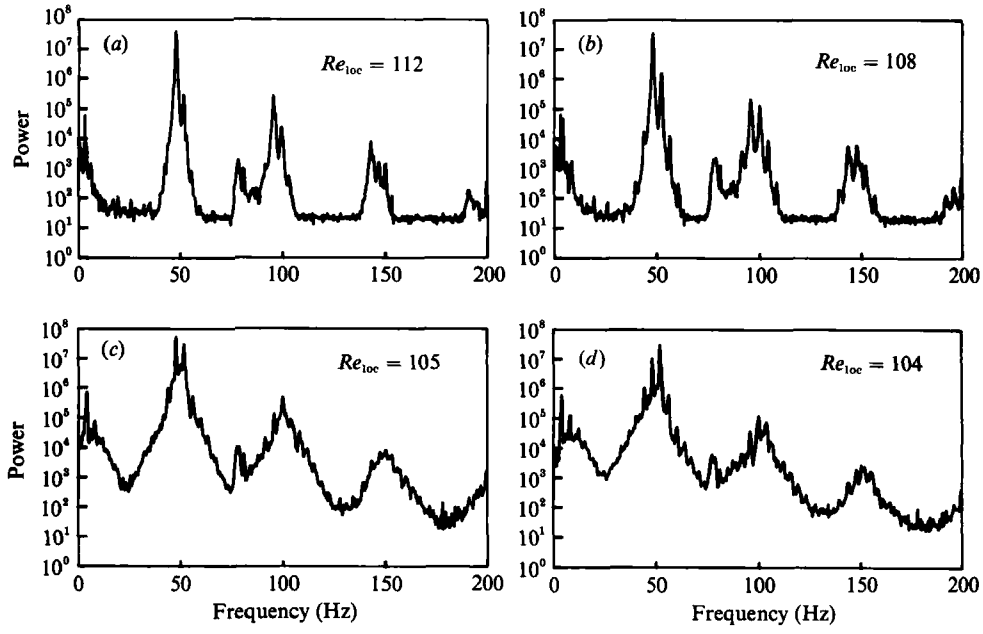

FIGURE 5. Power spectra at cellular Reynolds numbers ($Re \approx 100$). Cone C (*a*) $z = 45$ mm; (*b*) $z = 60$ mm; (*c*) $z = 75$ mm; (*d*) $z = 80$ mm.

frequency component present, and the modulation referred to in §3.1 is related to these broad peaks. Sharp spectral peaks at 100 Hz in figure 4(*b* and *c*) were due to mains interference and a weak signal generated by low Reynolds numbers. The vortex-shedding spectral peaks are much sharper in the cellular regime. At this stage it is again appropriate to clarify the concept of a cell. Although the power spectrum changes qualitatively along the span of the cone, there are extensive spanwise regions ('cells') in which the dominant frequency component of the spectrum is constant. Each such component is accompanied by several sideband frequency components, the upper sideband always being more dominant than the corresponding lower sideband, except in the immediate vicinity of a cell boundary. A modulating frequency, f_m, which is equal to the frequency difference, Δf, between the dominant frequency and its nearest sidebands, is also present in the spectrum. Figure 5 shows a series of power spectra as a cell boundary is approached and passed. Within the first cell (figure 5*a*) a dominant frequency is observed along with its upper sideband. As the cell boundary is approached along the span, the upper sideband becomes stronger and stronger (figure 5*b*, *c*), until there are two peaks of equal strength. At this point a cell boundary is defined. Then the formerly upper sideband becomes the new dominant frequency of the next cell, and the previous dominant frequency recedes and becomes the new lower sideband. This change-over is illustrated by figure 5(*c*, *d*). The same process occurs with the remaining cells, although there is a general broadening of the spectral peaks with increasing distance from the base. Thus the jump from one cell to another is associated with a continuous change in the spectrum, and does not arise from the disappearance of the old frequency and the sudden appearance of the new frequency. Consequently, it is not yet clear whether these cells are physical entities. When the cellular regime breaks down at higher Reynolds numbers, broad spectral peaks are observed again.

A very similar type of behaviour at cell boundaries has also been observed by

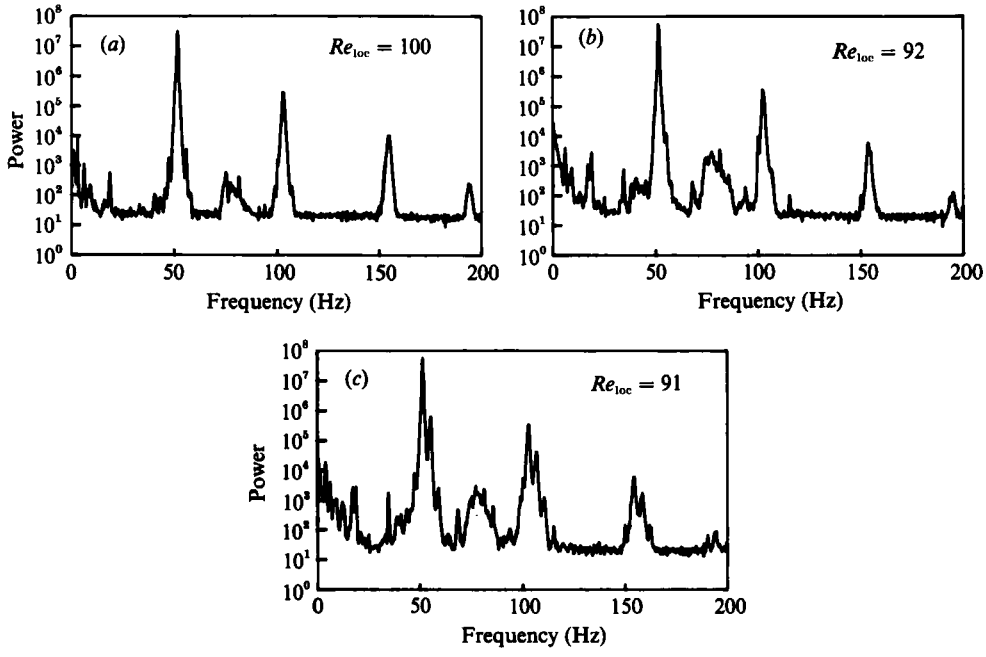

FIGURE 6. Power spectra at cellular Reynolds numbers ($Re \approx 100$) Cone A (*a*) $z = 50$ mm; (*b*) $z = 145$ mm; (*c*) $z = 160$ mm.

Williamson (1989), Gerich & Eckelmann (1982) and others for a circular cylinder. In these cases the boundary was usually between an end cell and the motion generated by the rest of the cylinder. The interaction at these boundaries has been attributed to a beating effect arising from the two separate (but close) frequencies of adjacent cells. However, experiments with single-cell cone A revealed more subtle behaviour. As with cone C above, a dominant frequency (surrounded by the usual sidebands) was present in the power spectrum. Figure 6 shows the variation of the power spectrum along the cone's length. It is apparent that the upper sideband increases in relative power along the cone, but never becomes dominant. If this sideband is taken to correspond to the frequency of the next cell, then it is significant that this frequency component is present even though the next cell does not exist. It seems probable that the modulating effect is intrinsic to the fluid mechanics of the system, and that the amplitude modulation is not due to a simple beating effect. This matter will be investigated more fully in §3.5.

3.4. *Frequency jump between adjacent cells*

Using cones with much higher taper angles than those employed in the present experiments, Gaster (1969) observed that the low-frequency modulation of the shedding frequency remained constant along the spans of his models. By non-dimensionalizing the modulating frequency, f_m, with the air speed, U, and kinematic viscosity, ν, he surmised that the quantity $f_m \nu/U^2$ was a constant. He also concluded that the modulating frequency was independent of any physical lengthscale of the model. Such a linear dependence on U^2 of the modulating frequency, f_m, or equivalently cellular frequency jump, Δf, was also observed in the present experiments, and the relation has been quantified. By assuming a relation of the form $\Delta f = k(U^2/\nu)$, values for the constant of proportionality, k (the 'Gaster'

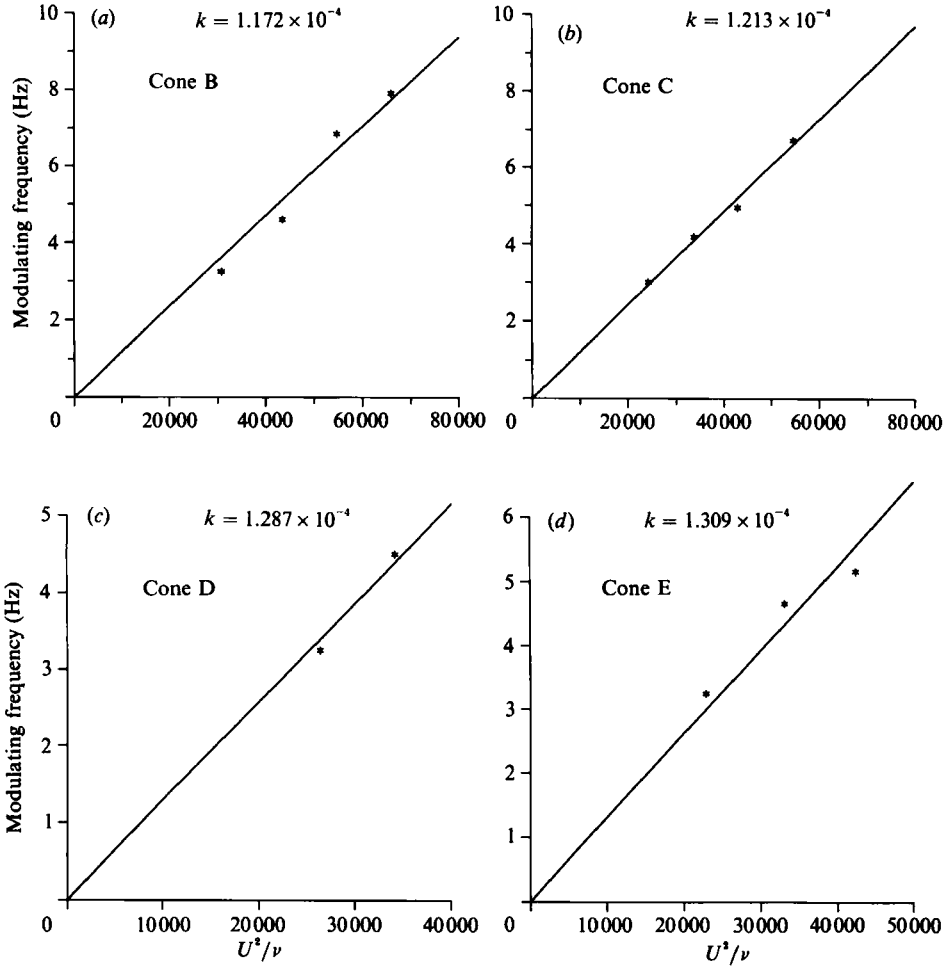

FIGURE 7. Variation of modulating frequency (or frequency jump) with U^2/ν. (*a*) Cone B; (*b*) Cone C; (*c*) Cone D; (*d*) Cone E.

constant), were determined for the cones. Figure 7 shows the results plotted for the different cones (except for the single-cell case of cone A, and the indistinct multiple-cell case of cone F), whilst figure 8 shows how k varies with the taper angle, α, of the cones.

3.5. *Complex demodulation*

The presence of multiple sidebands and related modulating frequencies in the power spectrum obtained from the vortex street suggested nonlinear behaviour, which could account for the strong interaction observed between the different frequencies in the system. The signals obtained were often strongly modulated in amplitude and it was not immediately clear whether this was due to the phenomenon of frequency beating (arising from the presence of two or more frequencies), or whether there was a genuine modulation process inherent in the system. The broadening of peaks observed in the power spectra may have been attributable to the simultaneous presence of frequency (or phase) modulation and amplitude modulation.

Miksad *et al.* (1982) conducted experiments in a forced two-dimensional laminar wake to observe and describe the amplitude and phase modulations, and their

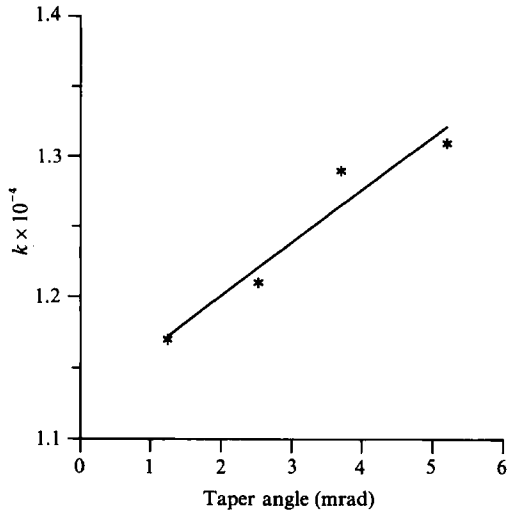

FIGURE 8. Variation of Gaster constant, k, ($\Delta f = kU^2/\nu$) with taper angle, α.

mutual interaction, during the transition to turbulence. Similar complex demodulation techniques were used to investigate the existence and nature of any amplitude and phase modulation of the present experimental signals.

Following Kim, Khadra & Powers (1980), a wave modulated in both phase and amplitude may be expressed as

$$\Phi(x,t) = a(x,t)\cos[k_0 x - \omega_0 t + p(x,t)],$$

where $a(x,t) = a_0 + a_m(x,t)$, and $a_m(x,t)$ and $p(x,t)$ are the amplitude and phase modulation respectively of a carrier wave with wavenumber k_0 and frequency ω_0. If this is multiplied by $2\exp(i\omega_d t)$, the following expression is obtained

$$2\Phi(x,t)\exp(i\omega_d t) = a(x,t)\{\exp[ik_0 x - i(\omega_0 - \omega_d)t + ip] + \exp[ik_0 x + i(\omega_0 + \omega_d)t - ip]\},$$

where ω_d is a demodulation frequency. There are two frequencies present now, corresponding to the sum and difference of ω_0 and ω_d. If ω_d is allowed to equal ω_0 and a low-pass filter is applied to cut off the sum frequency component, the complex demodulate

$$c(x,t) = a(x,t)\exp[ik_0 x + ip(x,t)]$$

is left. The amplitude of this demodulate describes the amplitude modulation of the carrier wave, whilst the phase part corresponds to the instantaneous phase modulation. The instantaneous frequency shift, $\delta\omega$, is given by the time derivative of the phase modulation:

$$\delta\omega = -\partial p/\partial t.$$

Kim *et al.* (1980) went on to show that the power difference between the nth upper and lower sidebands is mainly determined by the amplitude and phase modulation indices and the phase angle between the respective modulations.

Time series of the experimental signals were obtained, and, by identifying the modulation frequencies, ω_m, and carrier frequencies, ω_0, from the power spectra, the complex demodulate could be calculated. A cutoff frequency slightly higher than the modulating frequency was used. Figure 9 shows the time series of various signals

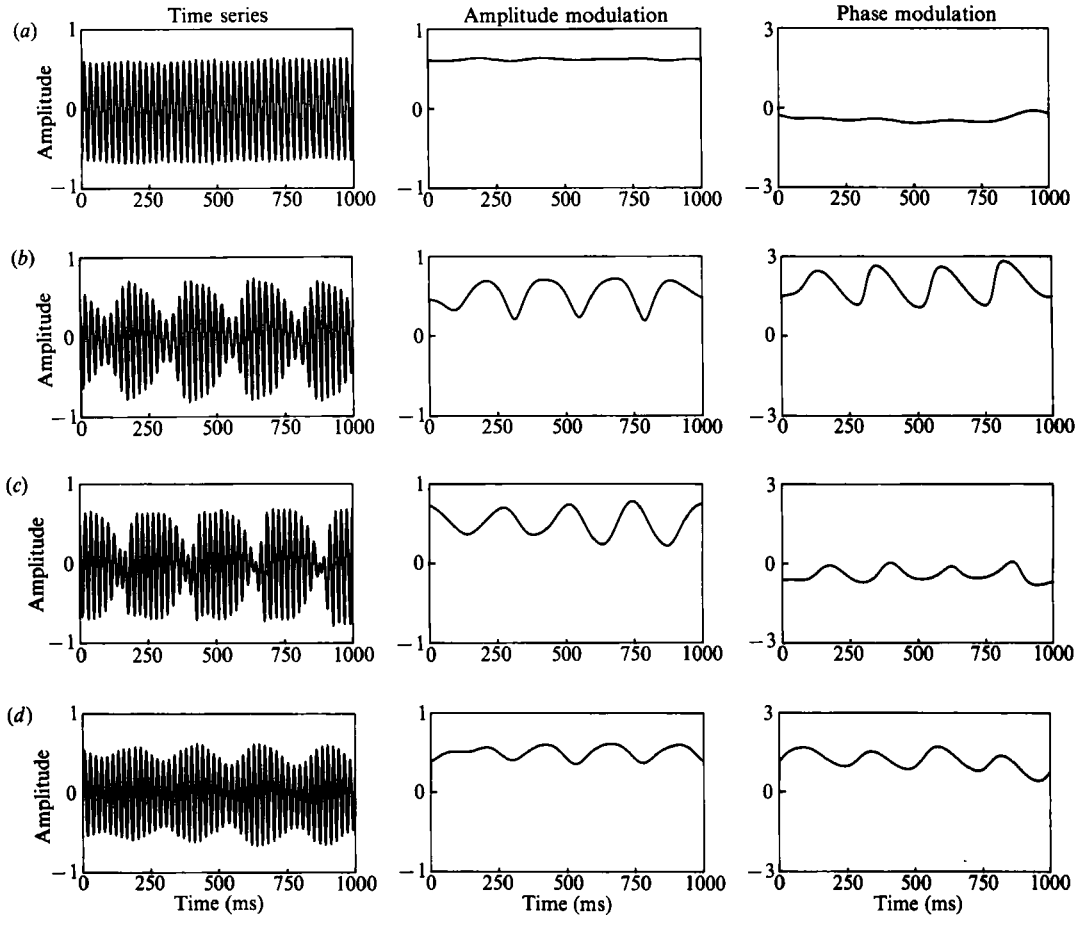

FIGURE 9. Time series, amplitude modulation and phase modulation for different signals. Cone C (*a*) $z = 50$ mm, $Re_{loc} = 104$; (*b*) $z = 100$ mm, $Re_{loc} = 92$; (*c*) $z = 110$ mm, $Re_{loc} = 90$; (*d*) $z = 125$ mm, $Re_{loc} = 87$.

with their respective amplitude and phase modulations. The offsets of the modulations have not been removed, so their mean is not zero. It is clear that both amplitude and phase modulation of the signal were present, suggesting that the signal is more complex than its appearance might otherwise suggest. The presence of significant phase (or frequency) modulation in the vicinity of a cell boundary results in a continually oscillating shedding frequency. It is important to emphasize that there is no particular unique shedding frequency associated with each cell, since the instantaneous frequency is continually changing.

The sign of the phase difference between the amplitude and phase modulation is related to the relative strengths of the lower and upper sidebands. For both cases, $z = 100$ mm and $z = 110$ mm (figure 9*b*, *c*), the amplitude modulation leads the phase modulation by about $\frac{1}{2}\pi$ radians. According to the analysis of Kim *et al.* (1980), this would be accompanied by an upper sideband that was stronger than the corresponding lower sideband. This was confirmed by the respective power spectra.

The results obtained support the theory that a modulating effect (probably related to the spanwise coupling), rather than a beating effect (arising from the interaction of two different frequencies), exists within the system.

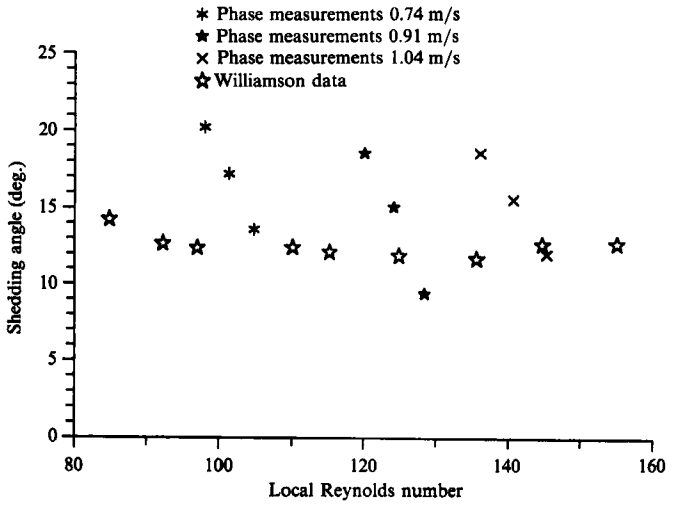

FIGURE 10. Shedding angles determined from phase measurements. Cone A.

3.6. *Shedding angle measurements*

In order to determine shedding angles, two probes spaced 15 mm apart in the spanwise direction were used. Williamson's (1989) method of observing Lissajous figures on an oscilloscope was inappropriate in the present experiments because of the much less steady and coherent nature of the vortices, and because of the presence of phase modulation.

The experimental technique involved the determination of the normalized cross-correlation coefficient, ρ_{xy}, between the two signals x and y, such that

$$\rho_{xy} = \frac{R_{xy}}{(R_{xx}R_{yy})^{\frac{1}{2}}}$$

(formed from the cross-correlation function, R_{xy}, and autocorrelation functions, R_{xx} and R_{yy}). By moving one probe relative to the other in the streamwise direction until the maximum of the above expression (ρ_{xy} as close as possible to 1) was achieved, the probes were assumed to be in phase. Simple geometrical arguments yielded the shedding angle. However, in order to improve accuracy, an averaging technique was employed. The value of ρ_{xy} was determined at twenty equally-spaced streamwise offsets of the two probes. The determination of the phase and frequency of a sine wave (of amplitude one) fitted to these data points yielded respectively the shedding angle and wavelength of the vortex lines. The technique proved to be very successful.

Shedding angles were obtained for cone A at three different pairs of spanwise locations ($z = 40/55$, $80/95$ and $120/135$ mm) at each of three different speeds ($U = 0.74$, 0.91 and 1.04 m/s). Spanwise locations greater than $z = 150$ mm produced less reliable data because of the increasing lack of coherency. The same difficulty arose with the other cones (with their smaller cells), and so only the results of cone A are presented in figure 10. Williamson's (1989) experimental data for the oblique shedding angles of a circular cylinder are also shown for comparison. A very similar trend to his was observed when a change in Reynolds number was caused by a change in speed. However, a change in Reynolds number arising from movement along the span (at constant air speed) resulted in a much larger variation in shedding angle. This was due to the spanwise coupling present within a cell. Such coupling would also account for the larger angles observed.

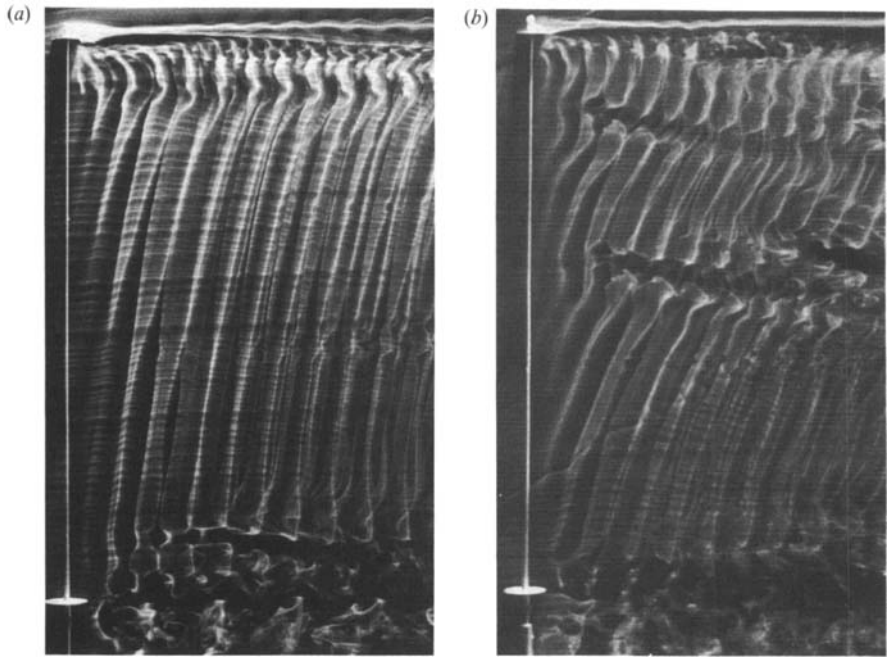

FIGURE 11. Flow visualization. Flow is from left to right. (*a*) Cone A, $Re_{max} \approx 100$; (*b*) Cone C, $Re_{max} \approx 140$.

Experiments with other cones showed that the shedding angle decreased across a cell boundary. It seems that the shedding angle is initially selected at the base of each cell and then increases rapidly (owing to the coupling) along the length of a cell. The shedding angle of the next cell begins at a lower value (probably determined by the local Reynolds number), but again increases rapidly. These observations suggest that the mechanism of shedding-angle selection, on a cone at least, may be more complicated than the mechanism proposed by Williamson (1989) for a cylinder, which involves the matching of end conditions along the span of the cylinder. Williamson's observation of only two unique shedding angles for a given Reynolds number (associated with a parallel mode and an oblique mode), despite variations in the alignment of the endplates, suggests that the selection of a shedding angle may be an internal process intrinsic to the system and that the angle is not necessarily exclusively determined by external boundary conditions.

According to Williamson (1989), the convection speed, U_c, of the vortices may be assumed to be independent of the shedding angle. Consequently, the streamwise separation of the vortex lines (wavelength, λ) is constant in a cell, since the frequency, f, is constant ($U_c = f\lambda$). Using knowledge of the wavelength, determined from the above data, convection speeds were found to be, typically, 90% of the free-stream speed, in good agreement with Williamson.

3.7. *Flow visualization*

Flow visualization of the models, which was conducted using a smoke-wire technique and apparatus described by Eisenlohr & Eckelmann (1989*a*), confirmed for the first time that the cells, which have so far been defined only on the basis of a most dominant frequency component, were real physical entities. Figure 11 shows the main features of the flow observed, with figure 11 (*a*) corresponding to (single-cell) cone A, and figure 11 (*b*) corresponding to (multiple-cell) cone C. The first observation

from the photographs is that the vortex lines are curved, with the shedding angle increasing towards the tip. Secondly, it is seen that the orientation and shape of the vortices is such that they first begin to peel from the tip and then the point of separation accelerates towards the base. Shedding angles were measured directly from the photographs taken supporting the values obtained in §3.6. When the cone length was shortened by moving the base endplate, the resulting new flow regime featured different shedding angles. A significant increase in the maximum shedding angle (measured at the tip of the cone) was observed when the length was shortened in this way. The flow regime did not, however, change with movement of the tip endplate. Again, the dominance of the largest local diameter was noted. The maximum shedding angles observed (about 30°) were of the same order as those offered by Noack *et al.* (1991) for their model. The usual vortex 'splitting' (as described by Eisenlohr & Eckelmann 1989*b*) or vortex 'dislocation' (Williamson 1989), may be seen in the multiple-cell configuration of figure 11(*b*). A decrease in shedding angle across a cell boundary was also observed. Periodic undulations, possibly related to the phase modulation, were also observed travelling along the span from the base to the tip.

Gaster & Ponsford (1984) investigated the flows over tapered flat plates at higher Reynolds numbers and observed a dependence of the flow features on the location of both the endplates. This is in contrast to the present experiments, which revealed the flow features to be independent of the tip endplate location. In addition, it is apparent from the photographs that the vortex lines begin to peel at the tip and not the base. This dominance of the base parameter remains unclear, but may be connected with the periodic undulations mentioned above.

4. Landau–Stuart model

4.1. *Introduction*

It was Gaster (1969) who first proposed the use of a nonlinear oscillator to model vortex shedding. His choice of oscillator was the van der Pol oscillator:

$$\frac{\mathrm{d}^2y}{\mathrm{d}t^2}+y=\epsilon(1-y^2)\frac{\mathrm{d}y}{\mathrm{d}t},$$

where ϵ, the nonlinear parameter, is small. To this he added a spanwise coupling term, of the form $\partial^2y/\partial z^2$, to account for the taper, and appropriate scaling factors to account for geometrical variations along the span.

More recently, Noack (1989) and Noack *et al.* (1991) investigated the behaviour of such a van der Pol oscillator but with a different coupling term assumed to arise from viscosity. The solution of this equation successfully modelled the presence of spanwise cells, but the coupling strength had to be greatly increased before an appropriate number of cells was observed. This suggests, not surprisingly, that some mechanism other than viscosity is responsible for the coupling. Slantwise shedding was also observed, along with power spectra consisting of dominant frequencies with sidebands.

Landau & Lifshitz (1959) showed how the stability of a steady flow investigated using a non-stationary perturbation could yield a third-order approximation to the Navier–Stokes equation, giving, for the amplitude variation of the speed u:

$$\frac{\mathrm{d}|u|}{\mathrm{d}t}=a|u|-b|u|^3 \quad (a, b \text{ constants}).$$

Following Provansal, Mathis & Boyer (1987), the complex form of this equation, the Landau–Stuart equation, will be used. This yields information about the amplitude and phase, and is given by:

$$\frac{du}{dt} = \sigma u - \tfrac{1}{2}l|u^2|u,$$

where σ and l are complex constants. If we denote the real and imaginary parts of σ and l by σ_r, l_r and σ_i, l_i respectively, and write $u = Ae^{-i\phi}$, then we may determine the two equations governing the amplitude and phase parts of the motion by equating the real and imaginary parts:

Amplitude:
$$\frac{dA}{dt} = \sigma_r A - \tfrac{1}{2}l_r A^3, \tag{1}$$

Phase:
$$\omega = \frac{d\phi}{dt} = \sigma_i - \tfrac{1}{2}l_i A^2. \tag{2}$$

Both Provansal *et al.* (1987) and Sreenivasan *et al.* (1987) confirmed the validity of these equations in describing the shedding characteristics of the flow past a cylinder near the critical Reynolds number, Re_c, but did not specify the range of validity of Reynolds number. Neither group mentioned the possibility of oblique shedding interfering with their results. However, it is highly unlikely that oblique shedding was present since only transients or acoustically-excited regimes were investigated, which result in parallel shedding.

Using the experimental results of Sreenivasan *et al.* (1987), appropriate values were determined for the complex coefficients σ and l, in terms of the viscosity, ν, the diameter, d, and the Reynolds number, Re. Their experiments showed that:

$$\sigma_r = (\nu/5d^2)(Re - Re_c), \tag{3}$$

$$\sigma_i = (\nu/d^2)[34.3 + 0.7(Re - Re_c)]. \tag{4}$$

At equilibrium, the amplitude, A, no longer varies with time,

$$\frac{dA}{dt} = 0,$$

and so, from (1)

$$\sigma_r A = \tfrac{1}{2}l_r A^3.$$

Experiments have shown that A^2 is proportional to $(Re - Re_c)$. If c^2 is the constant of proportionality, then we have:

$$A^2 = (\sigma_r/\tfrac{1}{2}l_r) = c^2(Re - Re_c).$$

If we determine c such that $A = 1$ at $(Re - Re_c) = 100$, then $c = 0.1$.
Substituting for σ_r from (3), we obtain:

$$l_r = 40(\nu/d^2). \tag{5}$$

At equilibrium, the frequency shift, $\Delta\omega = -\tfrac{1}{2}l_i A^2$ (see (2)), was found to vary as $0.1(Re - Re_c) \times (2\pi)$ by Sreenivasan *et al.* (1987). Setting $A^2 = \sigma_r/(\tfrac{1}{2}l_r)$ from above and equating, we obtain $l_i/l_r = -\pi$. Thus,

$$l_i = -126(\nu/d^2). \tag{6}$$

The natural shedding frequency at equilibrium observed by Sreenivasan *et al.* was given by

$$Ro = 0.21Re - 4.2$$

which is very similar to Roshko's line.

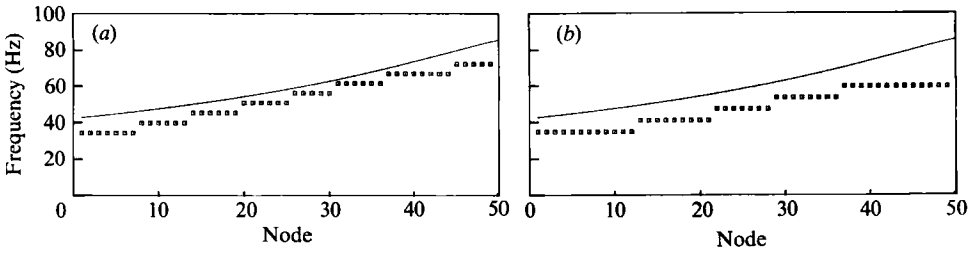

FIGURE 12. Spanwise variation of dominant shedding frequency component obtained from numerical simulations. $d_{max} = 3$ mm, $d_{min} = 1$ mm, $U = 0.7$ m/s. $Re_{max} = 144$. (*a*) $\lambda/(\Delta z)^2 = 250$; (*b*) $\lambda/(\Delta z)^2 = 500$. ——, 'natural' frequency.

In order to model the flow past a tapered body, some sort of spanwise coupling is necessary. Note that the complex coefficients, determined by the local diameter, vary along a tapered body. It is this that provides a 'natural' shedding frequency at each spanwise location. The addition of a spanwise diffusive term to act as the coupling mechanism results in a modified, partial differential equation:

$$\frac{\partial u}{\partial t} - \lambda \frac{\partial^2 u}{\partial z^2} = \sigma u - \tfrac{1}{2} l |u^2| u, \tag{7}$$

where λ is real and has the dimensions of viscosity. It is this equation that will form the basis of investigation as a mathematical model of the shedding of the cones. Following completion of the present work, it was learned that a similar model based on the Landau–Stuart equation has been proposed by Albarède, Provansal & Boyer (1990). Their model features a complex coupling coefficient.

Equation (7) may be expressed in a non-dimensional form using appropriate substitutions, though results are presented in dimensional form. By forming non-dimensional variables $u' = u/U$, $z' = z/l$, and $t' = \Omega t$, where U, l and Ω are respectively the free-stream speed, cone length, and shedding frequency at some reference point (the base, for example), a non-dimensional form for the coupling coefficient may be deduced, namely $\lambda' = \lambda/(\Omega l^2)$.

4.2. *Numerical procedure*

A centred, second-order-accurate finite-difference scheme for (7) was time-marched using a second-order Runge–Kutta method until an asymptotic state had been reached. The complex constants σ and l were determined at each of fifty spanwise nodes considered so that the mesh size, Δz, was 0.02. A mesh size of 0.01 was also investigated, but more timesteps were needed for stable convergence and the results were identical to those for a mesh size of 0.02. The kinematic viscosity, ν, was set at $\nu = 1.46 \times 10^{-5}$, and a critical Reynolds number, Re_c, of 46 (as determined by Sreenivasan *et al.* 1987) was employed. The Dirichlet boundary condition was imposed, enforcing a zero disturbance at the end nodes of the body to model the effect of the endplates in the experiments.

4.3. *Results*

It was immediately clear that spanwise cells could be generated by (7) for sufficiently large values of the coupling coefficient, λ. Specific values for $\lambda/(\Delta z)^2$, which were of the order of 500, are given in the relevant figures. Figure 12 shows a converged solution for two different coupling coefficients, an air speed of 0.7 m/s and end diameters of 3 and 1 mm. The solution was assumed to have converged once the

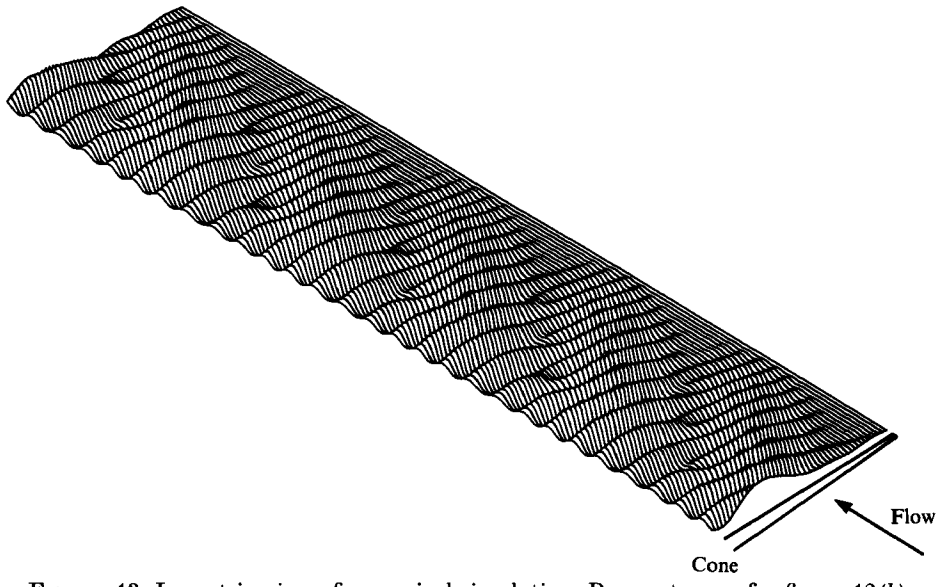

FIGURE 13. Isometric view of numerical simulation. Parameters as for figure 12(*b*).

frequency within each cell remained constant to at least four significant figures. A number of features determined from the experiments are observed. All the points are located below the uncoupled, 'natural' frequency, which is shown for comparison, and the frequency jump between adjacent cells is constant along the length of the cone. Both of these are important experimental features of the flow not supported by the model of Noack *et al.* (1991). An increase in coupling coefficient, λ, results in fewer cells. However, the trend of decreasing cell size with increasing spanwise location, observed in the experiments, is not observed in the simulations.

In order to achieve convergence at a particular mesh size, the timestep size, Δt, was reduced until the final, asymptotic solution had converged and shown no change with further reduction in Δt. A typical value for Δt was 10^{-4}. A formal stability analysis of the finite-difference equation was complicated by the nonlinear term in the differential equation. However, a sufficiently small timestep size ensured stable behaviour. It is worth mentioning that convergence began at the larger diameter end and progressed to the smaller diameter end. Convergence was more rapid when fewer cells were present.

Figure 13 shows an isometric view of the vortex structure formed by a typical numerical simulation. The mechanism of vortex splitting is apparent and the figure serves as a good illustration of how vortices interact at cell boundaries. This mechanism is very similar to that described by Williamson (1989) and Eisenlohr & Eckelmann (1989*a*, *b*) for the vortex splitting at the (experimental) cell boundaries of cylinders. A decrease in the amplitude of the oscillation with local diameter is also observed. The numerical simulations yielded vortices which were curved in such a way that the shedding angle within a cell increased with decreasing local diameter, a feature which was also identified in the flow visualization (see figure 11).

An increase in coupling coefficient (at constant speed and unchanged geometry) reduces the number of cells present and increases the frequency jump, Δf, between adjacent cells. It is interesting to note that the frequency of the first cell (nearest the base) remained almost constant despite changes in the coupling coefficient. This is reminiscent of the dominance of the base diameter observed in the experiments.

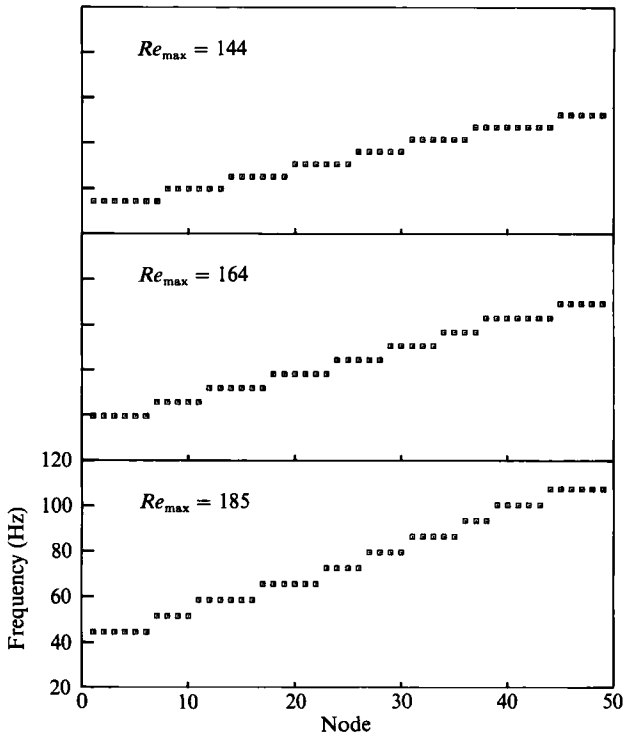

FIGURE 14. Variation of cellular arrangement with speed. $d_{max} = 3$ mm, $d_{min} = 1$ mm, $\lambda/(\Delta z)^2 = 250$. (*a*) $U = 0.7$ m/s; (*b*) $U = 0.8$ m/s; (*c*) $U = 0.9$ m/s.

The effect of an increase in air speed is shown in figure 14. Such an increase would lead to an increase in the reference shedding frequency, Ω, and this would reduce the non-dimensional coupling coefficient. The result was an increase in the number of cells and a larger frequency jump. The frequency jump was found to be proportional to the air speed at low coupling coefficients. The absence of this dependence at stronger coupling was probably attributable to the fewer cells present and the greater influence of the end conditions. The experimental dependence on air speed of the frequency jump, Δf, was found to be $\Delta f \propto U^2$, and an increase in air speed tended to reduce the number of cells present. This may suggest that the coupling coefficient, λ, and the coupling mechanism are both functions of the air speed. Experimental measurements showed an increase in both the maximum shedding angle and the modulating frequency strength with air speed (in addition to an increasing cell size), which also suggests an increase in coupling strength with speed. The frequency of the first cell in the numerical simulations was also found to be proportional to speed, and was not directly related to the 'natural' shedding frequency.

In order to determine the effect of a different taper angle on the system, two simulations with the same parameters except for a different tip diameter were performed. Figure 15 shows the results. It was important to keep the maximum (base) diameter fixed since this determined the first cell's frequency. A change in taper angle is equivalent to a change in l. The non-dimensional coupling coefficient, λ', is inversely proportional to l^2, so that an increase in taper angle (equivalent to a smaller l) would result in an increased λ'. In the region of local diameter 3 to 2 mm, the cone with the lower taper angle (figure 15*b*) supported more cells, but yielded a

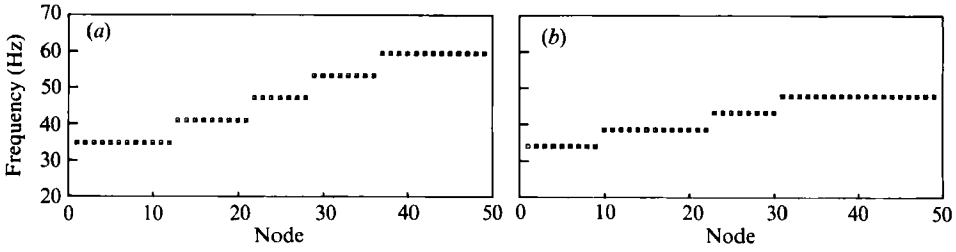

FIGURE 15. Variation of cellular arrangement with taper angle. $\lambda/(\Delta z)^2 = 500$, $U = 0.7$ m/s. $Re_{max} = 144$. (*a*) $d_{max} = 3$ mm, $d_{min} = 1$ mm; (*b*) $d_{max} = 3$ mm, $d_{min} = 2$ mm.

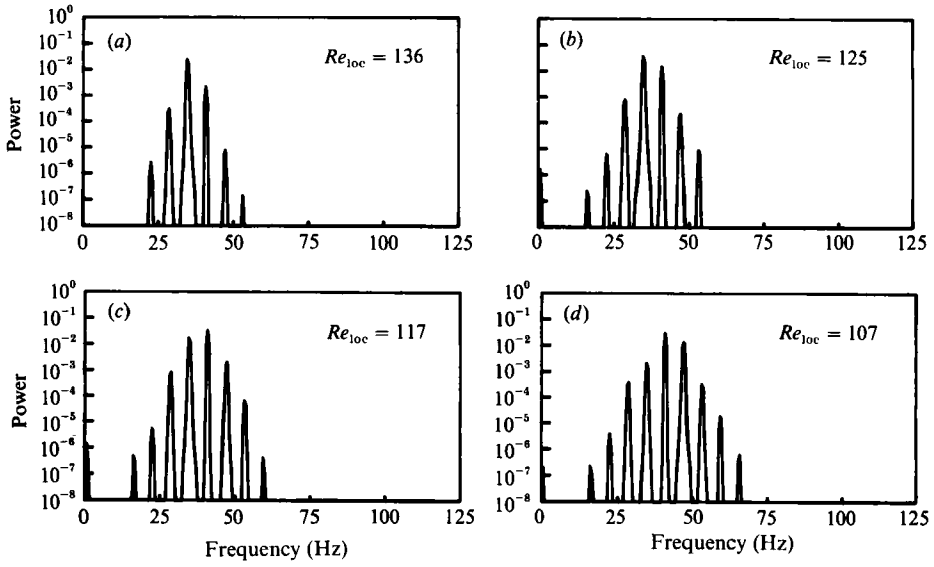

FIGURE 16. Power spectra at different spanwise nodes. $\lambda/(\Delta z)^2 = 500$, $U = 0.7$ m/s, $d_{max} = 3$ mm, $d_{min} = 1$ mm. (*a*) 4th node; (*b*) 10th node; (*c*) 14th node; (*d*) 19th node.

lower frequency jump. The effect of such a change in taper angle could not be investigated experimentally.

Typical power spectra are shown in figure 16. The nature of the spectra is very similar to those determined experimentally. A dominant frequency exists surrounded by equally spaced sidebands at multiples of the frequency jump between adjacent cells. It is interesting to note that the number of sidebands increases with node number, a trend which may be compared with the increasingly broader spectrum observed in the experiments. The absence of a modulating frequency corresponding to the frequency jump may also be noted.

The number of cells present was dependent on the coupling coefficient. Figure 17 shows the emergence of a new cell as the coupling coefficient is decreased. It is clear that the emergence of a new cell is a local and not a global event – at the instant of a cell's birth, the other cell boundaries and cell frequencies remain unaffected. It is only when this new cell grows that the cell boundaries gradually move and the cells adopt new frequencies. These observations are in agreement with those from the experiments (see §3.2).

The qualitative behaviour of the model has been shown to agree quite well with the experimental observations. In order for a more direct, quantitative comparison to be

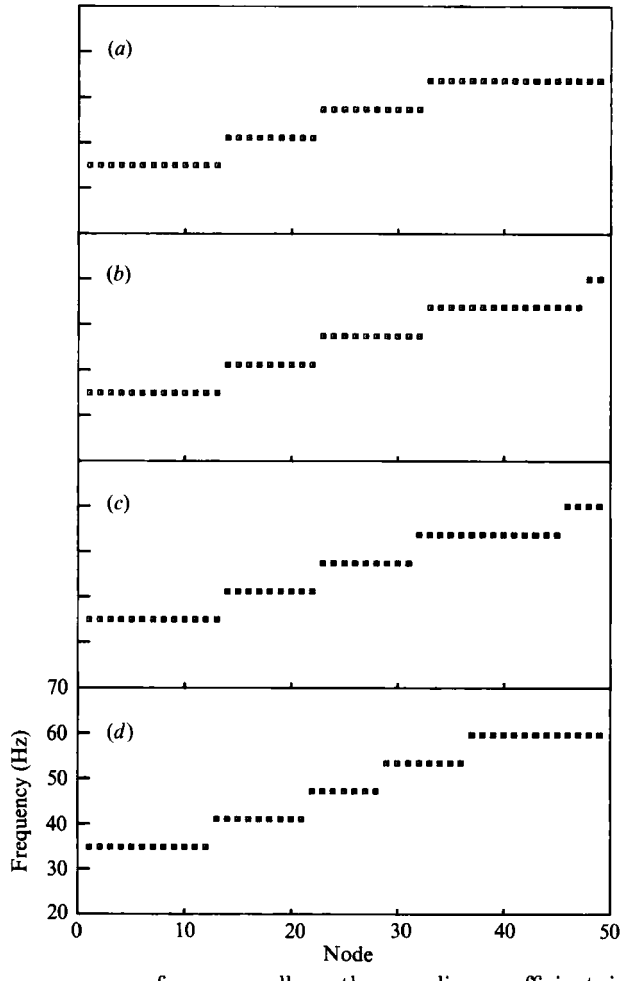

FIGURE 17. The emergence of a new cell as the coupling coefficient is varied. $U = 0.7$ m/s, $d_{max} = 3$ mm, $d_{min} = 1$ mm. $Re_{max} = 144$. (*a*) $\lambda/(\Delta z)^2 = 574$; (*b*) $\lambda/(\Delta z)^2 = 570$; (*c*) $\lambda/(\Delta z)^2 = 562$; (*d*) $\lambda/(\Delta z)^2 = 500$.

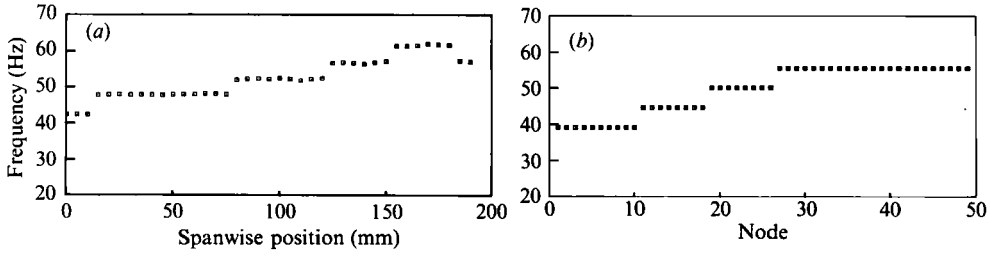

FIGURE 18. Comparison with experimental results. $d_{max} = 2.57$ mm, $d_{min} = 1.55$ mm, $U = 0.7$ m/s. $Re_{max} = 123$. (*a*) Experimental; (*b*) numerical ($\lambda/(\Delta z)^2 = 500$).

made, a simulation was conducted with parameters from an actual experiment. The dimensions of cone C were combined with an air speed of 0.7 m/s, and the experimental results of this configuration are shown in figure 18(*a*). The coupling coefficient was varied until the same number of cells was observed. Figure 18(*b*) shows the numerical results. Comparison with the experimental results shows that

the frequency jump is higher in the numerical simulation, while the frequencies of the cells are lower than those observed experimentally. The cell size does not decrease with increasing spanwise location as with the experiments. This may be related to the observation from the numerical simulations that the first cell's frequency was proportional to the air speed. If the frequency is not solely determined by the 'natural' shedding frequency, then the decreasing cell size trend (discussed in §3.2) would not necessarily be expected. It is also clear that end cells are not supported by the model. The shortcomings of the model are probably attributable to the choice of spanwise coupling. Barenblatt (private communication) has suggested that the coupling term might be improved by the addition of further terms of higher order.

5. Conclusions

The addition of a new parameter (the varying local diameter) to the classical problem of the flow past a circular cylinder has resulted in a flow which exhibits many new characteristics. The presence of spanwise coupling in the flow, a phenomenon not yet understood, leads to the formation of cells (regions of constant shedding frequency) at Reynolds numbers in the region of 100. The behaviour and characteristics of these cells have been investigated, and many similarities with the flow past a circular cylinder have been noted.

The mutual interactions between the coupling mechanism, the shedding mechanism, and the amplitude and phase modulations of the vortex shedding signal merit further investigation. It is possible that the modulated signals and oblique shedding angles observed are more intrinsic to the flow than has previously been suggested, and that they are not simply a result of the boundary conditions.

A mathematical model has been proposed for the system which has successfully modelled many, but not all, of the experimentally determined observations. It is possible that the diffusive term employed in the Landau–Stuart equation is not the most appropriate way of modelling the coupling mechanism.

The author is particularly grateful to Mike Gaster who inspired and supervised the work presented, which is a summary of Papangelou (1991). He is also indebted to Holger Eisenlohr for his assistance with the flow visualization of the cones, and to Bernd Noack for a continual and invaluable correspondence. Financial support from the Science and Engineering Research Council is gratefully acknowledged.

REFERENCES

Albarède, P., Provansal, M. & Boyer, L. 1990 Modélisation par l'équation de Ginzburg–Landau du sillage tridimensionnel d'un obstacle allongé. *C. R. Acad. Sci. Paris*, Ser. 2, **310**, 459.

Eisenlohr, H. & Eckelmann, H. 1989*a* Visualization of three-dimensional vortex splitting in the wake of a thin flat plate. *Proc. 5th Intl Symp. on Flow Visualization 21–25 August 1989* (ed. R. Reznicêk). Hemisphere, Washington, DC, USA.

Eisenlohr, H. & Eckelmann, H. 1989*b* Vortex splitting and its consequences in the vortex street wake of cylinders at low Reynolds number. *Phys. Fluids* A **1**, 189.

Gaster, M. 1969 Vortex shedding from slender cones at low Reynolds numbers. *J. Fluid Mech.* **38**, 565.

Gaster, M. 1971 Vortex shedding from circular cylinders at low Reynolds numbers. *J. Fluid Mech.* **46**, 749.

Gaster, M. & Ponsford, P. J. 1984 The flows over tapered flat plates normal to the stream. *Aeronaut. J.* **88**, 206.

GERICH, D. & ECKELMANN, H. 1982 Influence of end plates and free ends on the shedding frequency of circular cylinders. *J. Fluid Mech.* **122**, 109.

KIM, Y. C., KHADRA, L. & POWERS, E. J. 1980 Wave modulation in a non-linear dispersive medium. *Phys. Fluids* **23**, 2250.

KÖNIG, M., EISENLOHR, H. & ECKELMANN, H. 1990 The fine structure in the Strouhal–Reynolds number relationship of the laminar wake of a circular cylinder. *Phys. Fluids* A**2**, 1607.

LANDAU, L. D. & LIFSHITZ, E. M. 1959 *Fluid Mechanics*. Pergamon.

MIKSAD, R. W., JONES, F. L., POWERS, E. J., KIM, Y. C. & KHADRA, L. 1982 Experiments on the role of amplitude and phase modulations during transition to turbulence. *J. Fluid Mech.* **123**, 1.

NOACK, B. R. 1989 Untersuchung chaotischer Phänomene in der Nachlaufströmung eines Kreiszylinders. Diplomarbeit, Institut für Angewandte Mechanik und Strömungsphysik der Georg-August-Universität, Göttingen.

NOACK, B. R., OHLE, F. & ECKELMANN, H. 1991 On cell formation of vortex streets. *J. Fluid Mech.* **227**, 293.

PAPANGELOU, A. 1991 Vortex shedding from slender cones at low Reynolds numbers. PhD thesis, University of Cambridge.

PAPANGELOU, A. 1992 A 'robust' vortex-shedding anemometer. *Exps Fluids* (to appear).

PICCIRILLO, P. S. 1990 An experimental study of vortex shedding behind a linearly tapered cylinder at low Reynolds number. MS thesis, University of California, San Diego.

PROVANSAL, M., MATHIS, C. & BOYER, L. 1987 Bénard–von Kármán instability: transient and forced regimes. *J. Fluid Mech.* **182**, 1.

ROSHKO, A. 1954 On the development of turbulent wakes from vortex streets. *NACA Rep.* 1191.

SREENIVASAN, K. R., STRYKOWSKI, P. J. & OLINGER, D. J. 1987 On the Hopf bifurcation and Landau–Stuart constants associated with vortex 'shedding' behind circular cylinders. In *American Society for Mechanical Engineers Forum on Unsteady Flow Separation* (ed. K.N. Ghia), Fluids Engineering Division, vol. 52, p. 1. ASME.

WILLIAMSON, C. H. K. 1989 Oblique and parallel modes of vortex shedding in the wake of a circular cylinder at low Reynolds numbers. *J. Fluid Mech.* **206**, 579.